

Electrical and Electrochemical Properties of Sandwich- and Monolithic-Structured Dye-Sensitized Solar Cells with Various Counter Electrode Materials

Ellyse Oktaviani¹, Natalita M. Nursam^{2,*}, Shobih², Jojo Hidayat², Lia M. Pranoto², Erlyta S. Rosa², Niki Prastomo^{1,3}, Gerald E. Timuda⁴

¹ Department of Physics Engineering, Faculty of Engineering, Surya University, Tangerang, Banten – Indonesia

15143

² Research Center for Electronics and Telecommunication - Indonesian Institute of Sciences (LIPI), Bandung - Indonesia 40135

³ Department of Physics Engineering, Faculty of Engineering and Informatics, Universitas Multimedia Nusantara, Tangerang, Banten – Indonesia 15811

⁴ Research Center for Physics - Indonesian Institute of Sciences (LIPI), Tangerang Selatan, Banten – Indonesia 15314

*E-mail: natalita.maulani.nursam@lipi.go.id

Received: 10 May 2021 / Accepted: 1 July 2021 / Published: 10 August 2021

A counter electrode is one of the crucial components in dye-sensitized solar cell (DSSC), where platinum, carbon composite, and poly(3,4-dioxythiophene)-poly(styrene sulfonate) or PEDOT:PSS are among the most widely used materials. In terms of configuration, DSSC is typically constructed in two ways: sandwich and monolithic. However, the DSSC performance associated with the selection of both counter electrodes and configuration has received little attention to date. This study aims to study the effect of counter electrode materials on DSSC performance by analyzing their electrical and electrochemical properties from their configuration standpoint. First, the physical properties of the counter electrodes materials were analyzed using scanning electron microscopy (SEM), followed by four-point probes, electrochemical impedance spectroscopy (EIS), incident photon-to-current conversion efficiency (IPCE), and current density-voltage (J-V) characterization. Among all variations, our results show that the sandwich-type DSSC with PEDOT: PSS counter electrode generated the best performance with a power conversion efficiency of 5.40%, which was primarily attributed to the high conductivity (3210 S/cm) and low charge transfer resistance (R_{CE} 53 Ω). It was also found that the electron transfer pathways that are determined by the cell configuration also had a significant impact on the cell performance.

Keywords: counter electrode; dye-sensitized solar cell; electrical and electrochemical properties; monolithic; sandwich

1. INTRODUCTION

Dye-sensitized solar cell (DSSC) is a third-generation photovoltaic device that has been considered a promising alternative to the conventional first-generation silicon-based solar cells [1]. The charge generation mechanism used by DSSC is modeled after the photosynthesis process. Owing to its low production cost, simple fabrication, and low susceptibility to defects, DSSC has drawn major interest both in the academic and industrial community [2, 3].

A sandwich-type DSSC consists of two transparent conducting oxides (TCO) substrates, one of which contains a layer of a wide bandgap semiconductor that has been sensitized with dye molecules and is referred to as the working electrode, and the other of which is coated with a catalyst layer and is referred to as the counter electrode. To reduce the oxidized dye sensitizer, an electrolyte solution containing redox mediator is injected between the two electrodes [4]. The application of two TCO in a sandwich-type DSSC has often become a major predicament in reducing the total material cost in the fabrication of DSSC. This is primarily because the cost of TCO substrate accounts for approximately 60% of the total materials cost in DSSC [5]. Thus, an alternative configuration so-called “monolithic” is often sought-after to replace the conventional sandwich structure. A monolithic-type DSSC typically consists of a photoelectrode layer, spacer, and counter electrode that are stacked on a single TCO substrate [6].

One of the main components in DSSC is a counter electrode. The counter electrode functions as a positive electrode, collecting electrons that have passed through the external load and also acts as a reflector that reflects the unabsorbed light into the active area of the cell [7]. The reduction reaction between the transferred electron received at the counter electrode and the triiodide within the electrolyte and ($I_3^- + 2e \rightarrow 3I^-$) occurs slowly, thereby often ends up in charge transfer overpotential [8]. Adding a catalyst layer in the counter electrode is therefore required to accelerate such a reaction. Given its importance, an ideal counter electrode should be chemically, mechanically, and electrochemically stable, as well as have an energy level that matches the electrolyte redox couple potential with good catalytic activity, reflectivity, high porosity, high surface area, high adhesivity with TCO substrate, and preferably have low material cost [9].

Platinum has been frequently used as a counter electrode material in DSSC, owing to its high catalytic activity with I_3^-/I^- , which is the most employed redox couple in electrolyte for DSSC to date [10]. However, the expensive cost and the limited supply of this material have somewhat hindered the commercial application of DSSC. As a result, considerable effort has been devoted to the search for alternative materials. Two material candidates that are less expensive than platinum with a competitive catalytic performance suitable for the counter electrode in DSSC are carbon and poly(3,4-ethylene dioxythiophene) polystyrene sulfonate (PEDOT:PSS) [11]. Carbon is one of the most abundant materials on earth. Carbon also has high catalytic activity, porous, corrosion-resistant, high surface area, and most importantly, less expensive than metals. A previous study reported that the use of carbon as a counter electrode in a monolithic DSSC produced better solar cell performance than that of sputter-coated platinum [12]. Carbon materials, particularly graphite and activated carbon, are often applied as counter electrodes in DSSC. Graphite is a crystalline form of carbon with high electrical conductivity but a large particle size, resulting in a low surface area and thus a lower reduction rate of I_3^- to I^- [13]. In contrast,

activated carbon is an amorphous form of carbon that is highly porous (i.e. microporous) and has a large surface area but low conductivity [14]. A previous study reported that combining graphite and activated carbon with an optimum composition ratio of 1:4 produced a relatively high power conversion efficiency (PCE) in monolithic DSSC [15]. In addition to carbon, PEDOT:PSS is a material of great interest for many electronic devices, including solar cells. PEDOT:PSS is a conductive polymer with high catalytic activity, high electrical conductivity (up to 1000 S/cm), flexibility, transparency, high stability, low cost, and could be straightaway deposited as a thin film [16]. The water-soluble characteristics of PEDOT:PSS makes it easy to produce and the industry's most widely used polymer [9].

There have been several studies reported on the fabrication of DSSC using a counter electrode made of platinum, carbon, and PEDOT:PSS [17–28]. However, there is still a lack of sufficient study to date that reports a thorough comparison on the performance of DSSC with those materials as counter electrodes using both sandwich and monolithic configuration prepared under equal conditions. In this study, we will analyze the performance of DSSCs with various counter electrodes (i.e. platinum, carbon, and PEDOT:PSS) with respect to the cell configuration (i.e. sandwich and monolithic) that were prepared using the same materials and under the same fabrication conditions. A detailed study on the electrochemical properties of the above variations will be reported herein to understand the physical mechanism that eventually determines the electrical output. The comparative study performed in this study could be used as a consideration in improving the cell performance in the future by selecting suitable counter electrode material that can work best depending on the cell configuration.

2. EXPERIMENTAL

2.1. Materials

All materials were used as obtained without any additional modifications. The following are the materials used in this experiment: fluorine-doped tin oxide (FTO) conductive glass substrates with a sheet resistance of $15\Omega/\text{sq}$ (Greatcell TEC-15), TiO_2 blocking layer paste (Greatcell BL-1), TiO_2 nanoparticle paste (Greatcell 18NR-AO), Ru-based dye-sensitizer Z907 (Greatcell), TiCl_4 (Merck, synthesis grade), ZrO_2 paste (Solaronix, Zr-Nanoxide Z/SP), iodide-triiodide based liquid electrolyte (Greatcell, EL-HPE), thermoplastic sealant (SurlynTM), deionized water, isopropyl alcohol (Bratachem), Teepol (Bratachem), aluminum foil, silver conductive pen, and silicon rubber (Dexton). As for the counter electrode, platinum and PEDOT:PSS paste were purchased from Greatcell (PT1) and Agfa (AGFA EL-P 505), respectively, while the carbon composite paste was prepared by mixing 0.5 g of graphite flake (Sigma Aldrich), 2 g of activated carbon, 0.25 g of TiO_2 (Degussa P25), 4.25 g of α -terpineol (Sigma Aldrich), and 0.3 g of hydroxyethyl cellulose (Merck Schuchard OHG) following an optimum composition from the previous study by [15]. All of the ingredients were ground, stirred, and mixed in a mortar until a paste with good consistency was obtained.

2.2. Device Fabrication

Initially, FTO substrates were cut into two sizes, i.e. $15 \times 1 \text{ mm}^2$ for sandwich DSSC and $20 \times 15 \text{ mm}^2$ for monolithic DSSC. In monolithic DSSC, the anode and cathode are situated on the same

conductive substrate, thus electrode separation was performed by removing the conductive layer between them. All of the FTO glass substrates, both with and without scribing, were then cleaned by ultrasonication in Teepol™, deionized (DI) water, and isopropyl alcohol (IPA), consecutively, for 10 min for each step.

The working electrodes were prepared following the procedure in previous reports [28–30]. First, the TiO₂ blocking layer was deposited on the FTO substrate using the screen printing method with a 200T mesh screen. The coated substrates were subsequently dried in an oven at 120 °C for 10 min and annealed in a furnace at 500 °C for 30 min. Subsequently, the samples were coated with TiO₂ nanoparticles via screen printing method with a printing area of 0.5 × 0.5 cm². The TiO₂ film was deposited twice to obtain a film with a thickness of approximately 10 μm. After each deposition, the samples were dried in an oven at 120 °C for 10 min before being annealed in a furnace at 500 °C for 30 min.

All samples were then post-treated by immersing in 40 mM of TiCl₄ solution at 70 °C for 30 min, followed by annealing at 500 °C for 30 min. The deposition of the ZrO₂ layer was only performed on monolithic DSSC as it requires an insulating spacer layer to separate both electrodes. Meanwhile, the electrodes in the sandwich DSSC were separated using a thermoplastic sealant that also serves as a spacer. Similar to TiO₂, the ZrO₂ layer was deposited twice, dried in an oven at 120 °C for 10 min after each deposition, and then annealed at 450 °C for 25 min.

The counter electrodes were fabricated by depositing either platinum, carbon composite, or PEDOT:PSS paste on top of the FTO substrate using a screen printing method. For sandwich DSSC, the counter electrode was prepared by printing the catalyst materials separately on the top of a bare FTO substrate. Meanwhile, for the monolithic DSSC, the catalyst layer was deposited on the FTO substrate that has been previously coated with TiO₂ and ZrO₂. The catalyst materials were repeatedly deposited to obtain layers with a similar thickness of 10 μm. The platinum and carbon composite films were dried in an oven at 120 °C for 10 min after each deposition, while PEDOT:PSS films were dried in a hotplate at 70 °C for 10 min. All platinum and carbon composite samples were then annealed in a furnace at 450 °C for 30 min, while PEDOT:PSS samples were annealed at 120 °C for 30 min.

A dye solution was prepared by dissolving 0.02 g of cis-Bis(isothiocyanato) (2,2'-bipyridyl-4,4'-dicarboxylato) 4,4'-dinonyl-2'-bipyridyl)ruthenium(II) (namely Z-907) dye on 100 ml ethanol. The dissolving process was performed by ultrasonication for at least 10 min. The sensitization was performed by immersion in the dye solution at room temperature under dark conditions for 24 h. Note that the immersion for sandwich DSSC was performed on photoanodes containing only the TiO₂ layer, while the immersion for monolithic DSSC was performed on the whole-cell that contains photoanode TiO₂, ZrO₂, and counter electrode. Upon completion, all samples were rinsed with ethanol and dried in the air.

For the DSSC with sandwich configuration, the photoanode and counter electrode were assembled in a sandwich-like structure using thermoplastic sealant (Surlyn™) and pressed at 120 °C to strengthen the bond between the substrates. Then electrolyte was then injected into the cell through a gap between two electrodes. Finally, the remaining gap in the constructed cells was encapsulated with silicon rubber. The substrates for the DSSC with monolithic configuration were assembled by covering the cell with a non-conductive glass that contains a pre-drilled hole. The electrolyte was injected into the cell through the hole, and the hole was then encapsulated with silicon rubber. The final configuration of

layers for both sandwich and monolithic DSSC are depicted in Figure 1. Before solar cell characterization, an additional silver film was coated onto each electrode to provide good electrical contact.

2.3. Characterizations

The surface morphology of the counter electrode was observed using a 20 kV scanning electron microscope (SEM) JEOL JSM-IT 300. All samples were sputter-coated with Au before the SEM analysis. A four-point probe HP 3468A multimeter was used to measure the sheet resistance of the counter electrodes. The current-voltage of the constructed cells was measured using the National Instrument I-V measurement system to study the electrical properties of DSSC. All of the I-V measurements were performed at room temperature under a sun simulator (Oriol) with an AM 1.5 G filter and an intensity equal to 1 Sun. The external quantum efficiency of the DSSC cell was characterized using the incident photon-to-current conversion efficiency (IPCE) measurement system (Newport 2636-R). The internal resistances at the solar cell interfaces were measured using electrochemical impedance spectroscopy (EIS) with a potentiostat (Gamry Ref3000) under illumination with a frequency range 0.01 Hz to 35000 Hz.

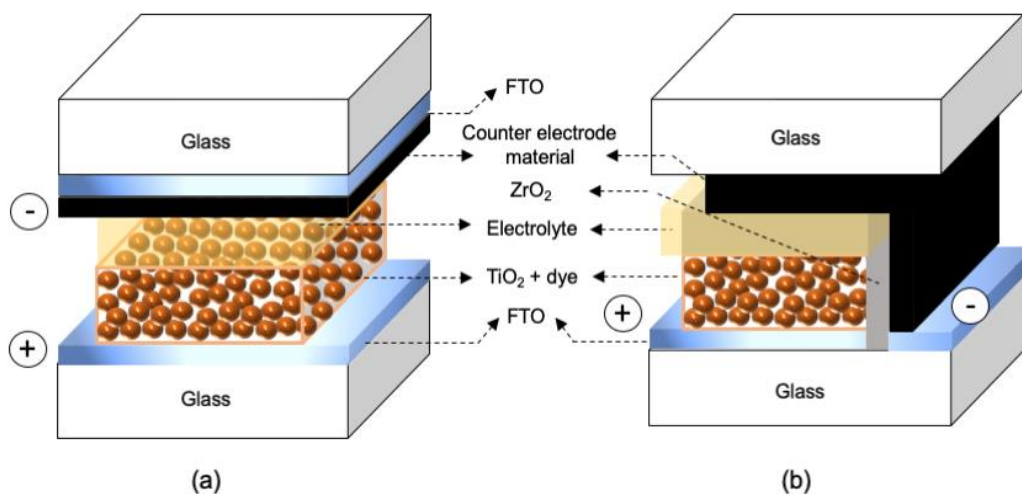


Figure 1. Schematic image of DSSC with (a) sandwich and (b) monolithic configuration.

3. RESULTS AND DISCUSSION

The final sandwich and monolithic DSSC prototypes with various counter electrode materials are shown in Figure 2. It should be noted that to ensure a fair comparison, both the sandwich and monolithic DSSC constructed in this study had the same active area with a size of 0.25 cm^2 . The area where the working and counter electrodes overlap was used to determine the active area.

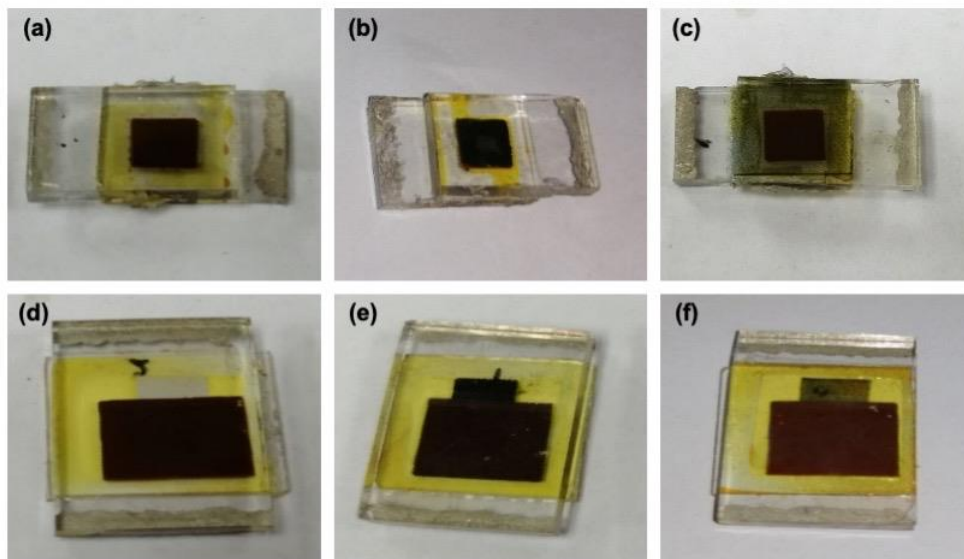


Figure 2. Photograph of (a-c) sandwich- and (d-f) monolithic-type DSSC with the counter (a and d) platinum, (b and e) carbon composite, and (c and f) PEDOT:PSS counter electrode.

Figure 3(a)-(c) shows the surface morphologies of platinum, carbon, and PEDOT:PSS counter electrodes. Figure 3(a) shows that the platinum layer is composed of relatively uniform submicrometer particles. Meanwhile, the surface morphology of carbon shown in Figure 3(b) displayed the surface morphology of carbon composite with a mixture of large particles of various sizes. The inhomogeneous particle size distribution shown by the carbon counter electrode is likely due to the presence of various elements that made up the carbon composite. The large size particles, for instance, belongs to the graphite flakes, while the small particles that existed between the large aggregates corresponded to the activated carbon and TiO_2 particles within the paste. TiO_2 P25 nanoparticles served as a binder that connects the carbon particles, and also as an adhesive to strengthen the bonding of the carbon composite layer onto the FTO substrate [31]. Figure 3(d) and 3(e) shows the SEM image of pristine graphite and activated carbon, respectively, which were used as the main components to make the carbon composite paste. The SEM images show that the activated carbon exists as agglomerations of small particles with abundant interparticle pores in between, while the graphite has a non-porous flake-like morphology with uneven sizes, i.e. up to tens of micrometer. These individual SEM images suggest that it is understandably difficult to obtain a smooth layer of carbon composite with uniform particle size, as confirmed by Figure 3(b). On the contrary, the morphology of the PEDOT:PSS layer shown in Figure 3(c) had a smoother surface than platinum and carbon composite with better uniformity and surface coverage. In this layer, holes, and pores are hardly visible among the particles. For monolithic-type DSSC, the smooth morphology of PEDOT:PSS could be particularly undesirable because it may provide fewer pathways for the penetration of electrolytes, thereby causing slower reduction. To improve the roughness of PEDOT:PSS, a mixture of PEDOT:PSS with rougher materials such as carbon [32], silicon nanoparticle [33], or titanium disulfide [34] have been reported. However, since we herein aim to compare the effectiveness of pure catalyst materials as counter electrodes in sandwich and monolithic DSSC, such modifications were not performed in this study.

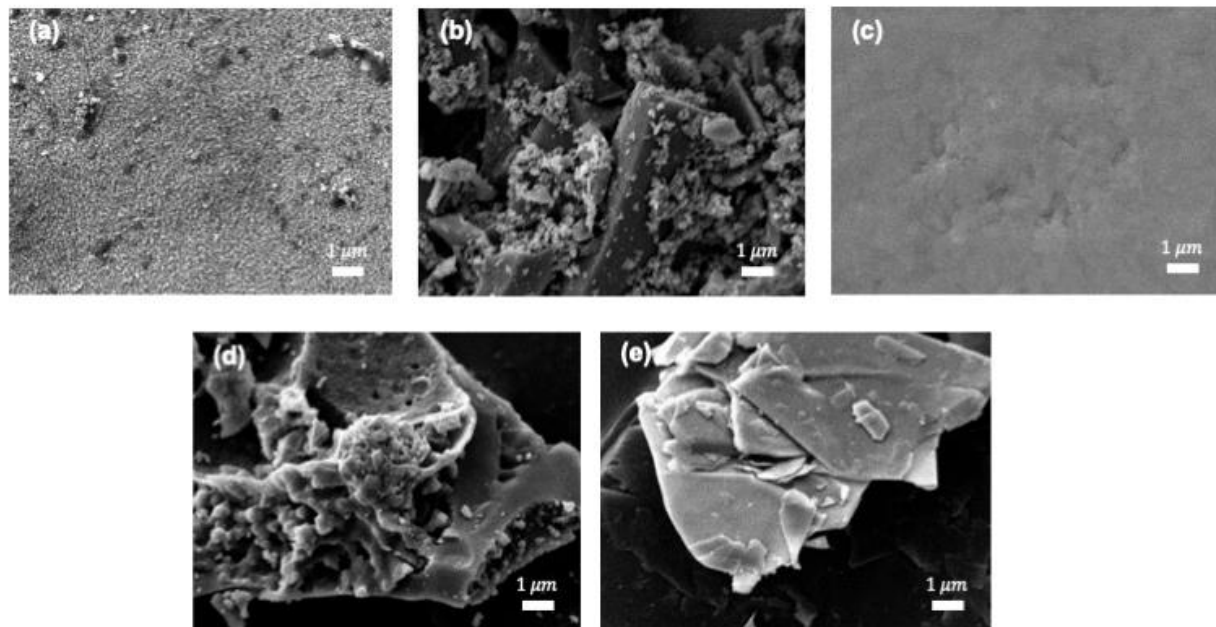


Figure 3. SEM images of (a) platinum, (b) carbon composite, and (c) PEDOT:PSS counter electrode. The SEM images of (d) activated carbon and (e) graphite are provided to show the main materials used to make up the carbon composite counter electrode shown in (b).

The sheet resistance of a counter electrode contributes to the parasitic resistances in DSSC, which in turn affect the fill factor, maximum power, and ultimately the power conversion efficiency of DSSC. To obtain a high fill factor, the resistivity of the counter electrode must be kept as low as possible [35]. The average sheet resistance of platinum, carbon, and PEDOT:PSS layer are provided in Table 1. According to Wu *et al.*, the resistivity of a counter electrode ideally should be less than 20 Ω/sq [9]. Our results indicate that platinum, carbon, and PEDOT:PSS could be applied as an ideal counter electrode for DSSC.

The conductivity of a counter electrode is related to the ability of the counter electrode to transfer electrons. The higher the conductivity the better the counter electrode transmits electrons. Below is the equation used to convert sheet resistance value into conductivity value:

$$\sigma = \frac{1}{R_s t} \times 100\% \quad (1)$$

where σ is conductivity (S/cm), R_s is sheet resistance (Ω/sq), and t is layer thickness (cm). The average conductivity of platinum, carbon, and PEDOT:PSS counter electrode is 600, 1636, and 3210 S/cm, respectively. PEDOT:PSS shows the highest conductivity than the other two counter electrodes, suggesting that PEDOT:PSS had the best electron transfer ability compared with the platinum and carbon composite. The high conductivity of PEDOT:PSS is possibly attributed to its morphology. The particle structure of PEDOT:PSS showed in Figure 3(c) is similar to those reported in previous studies that showed interconnected and tightly arranged particles, thus giving small surface area and smooth surface morphology [34, 36]. The interconnected particles of PEDOT:PSS also causes good contact between the particles, thereby facilitating the transport of electrons through the material [37]. Despite having a small particle size similar to PEDOT:PSS, platinum had a rough surface morphology, indicating that it had a

large surface area but with less interconnected particles. The gaps between the platinum particles cause low electron transport, thus decreasing the electrical conductivity of platinum.

Table 1. The resistivity and conductivity of various counter electrodes.

Parameter	Platinum	Carbon	PEDOT:PSS
Sheet resistance (ohm/sq)	14.3 ± 0.3	8.7 ± 0.3	3.1 ± 0.4
Conductivity (S/cm)	698 ± 10.9	1636 ± 54.9	3410 ± 232.3

From the EIS characterization, a Nyquist plot depicting the relationship between Z (real impedance) and Z'' (imaginary impedance) was obtained and shown in Figure 4. The EIS of DSSC typically shows three semicircles [39, 40]. It can be seen in Figure 4 that each DSSC variation has a different semicircle size, shape, and position. The semicircles of sandwich-type DSSCs regardless of the counter electrode materials used are located closer to the zero points of the Z' axis of the graph than the semicircles of monolithic DSSCs. This phenomenon shows that the DSSC with monolithic configuration produced higher series resistance than the DSSC with sandwich configuration. Meanwhile, the width and the height of the semicircles in the Nyquist plot are related to the resistance and capacitance, respectively. Figure 4 shows that the second semicircle has the most pronounced difference between each variation of DSSC. This suggests that the configuration and material used in the counter electrode of DSSC have a significant effect on the impedance (i.e. resistance and capacitance) in TiO_2 and therefore will significantly affect the activity of the electron in TiO_2 .

An equivalent circuit shown in Figure 5 was used to obtain a good fitting for the EIS parameters to study the electron transport and recombination in DSSC. It should be noted that in monolithic DSSCs, ZrO_2 was used as an additional material that serves as a spacer layer to separate the TiO_2 and dye from the counter electrode. ZrO_2 has a large bandgap of 6 eV, which is almost twice as large as the TiO_2 bandgap, and thus has high insulation properties that prevent electron transfer between the counter electrode and ZrO_2 , TiO_2 , and ZrO_2 , or between the ZrO_2 particles themselves [38]. Although the monolithic DSSC has an additional layer of ZrO_2 , the electrolyte that involves in the electrons transport from the counter electrode to the dye and TiO_2 is located within the pores of ZrO_2 , hence the working principles between monolithic DSSC and sandwich DSSC are the same. Thus, the equivalent circuit used for both monolithic DSSC and sandwich DSSC is the same [13]. The EIS parameters obtained from the fitting are shown in Table 2.

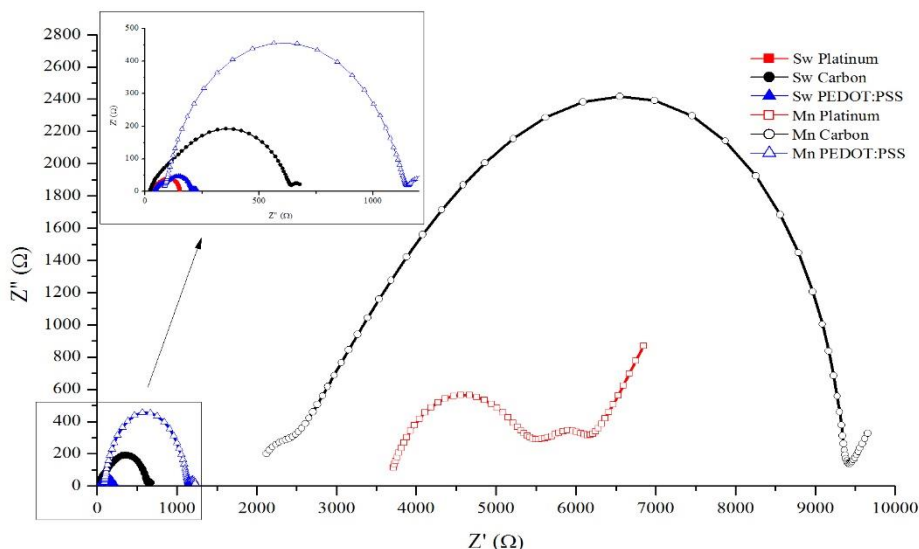


Figure 4. Nyquist plot obtained from sandwich- (Sw) and monolithic-type (Mn) DSSC with platinum, carbon, and PEDOT:PSS counter electrode.

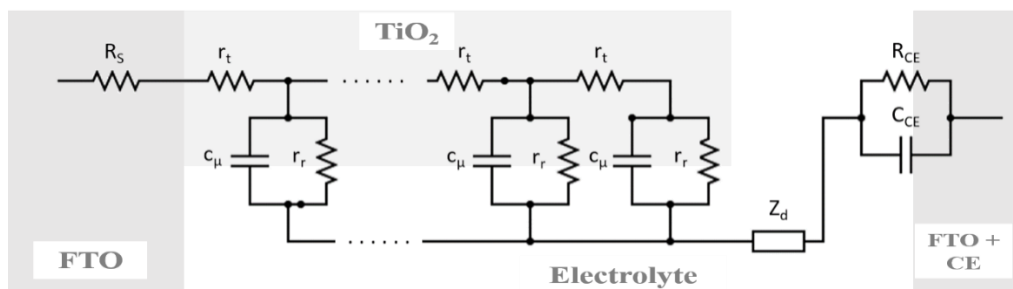


Figure 5. The equivalent circuit model used to fit the impedance spectra of DSSC.

Table 2. Impedance parameters obtained from electroimpedance measurement.

DSSC and CE type	R_s (Ω)	R_{CE} (Ω)	C_{CE} (μF)	R_t (Ω)	R_r (Ω)	C_μ (μF)	R_d (Ω)	τ_{tr} (ms)	L_n (μm)
Sw Platinum	29.5	58.4	20.6	3.9	58.1	88	32.9	0.4	38.2
Sw Carbon	22.1	102	5.2	4.7×10^{-2}	510	20.7	55.1	9.8×10^{-4}	1035.1
Sw PEDOT:PSS	21.6	53	3.06	4.1×10^{-2}	111	44.3	20.5	1.8×10^{-4}	1643.4
Mn Platinum	3640	1750	10.34	845	353	804	2.0×10^{-4}	679.4	6.5
Mn Carbon	1900	3170	2.79	15900	1200	10.5	4.6×10^{-4}	166.6	2.8
Mn PEDOT:PSS	65.9	738	1.05	66.2	317	3.1	93.6	0.2	21.9

R_s : series resistance; R_{CE} : charge transfer resistance at the counter electrode/electrolyte; C_{CE} : charge transfer capacitance at the counter electrode/electrolyte; R_t : electrons transport resistance in TiO_2 ; R_r : recombination resistance at the dye/ TiO_2 /electrolyte; C_μ : capacitance at the TiO_2 ; R_d : diffusion resistance at the electrolyte; τ_{tr} : electron transport time; L_n : electron diffusion length.*

No significant difference was observed among the R_s values of sandwich-type DSSC with various counter electrode materials. This phenomenon is likely linked to the electrons transfer in sandwich-type DSSC that is mostly occurred in the FTO substrate. Thus, the R_s value does not vary significantly due to the same resistivity used in the FTO substrates for all counter electrode variations. Meanwhile, the overall R_s values of monolithic-type DSSC are substantially higher than the R_s of sandwich-type DSSC. The higher R_s values in monolithic DSSC are primarily attributed to the large area of the catalyst materials that are not in direct contact with the conductive substrate, thus causing low lateral conductivity and affecting the length of the electron pathways. This is typically indicated by the limited ohmic resistance at the electrolyte and counter electrode interface [41]. Consequently, the R_s value of monolithic-type DSSC is more highly dependent on the sheet resistance of the counter electrode (see Table 1), whereas it is more negligible in the sandwich-type DSSC. Hence, the R_s of monolithic-type DSSC with PEDOT:PSS counter electrode is the lowest because the sheet resistance of PEDOT:PSS counter electrode is the lowest among the other counter electrodes, and vice versa for the platinum counter electrode.

It also noteworthy that the R_s value for monolithic-type DSSC with PEDOT:PSS is only 1.6 times higher than that of sandwich, while the other counter electrodes show pronounced differences (i.e. the R_s for platinum and carbon in monolithic-type DSSC was 123 and 86 times higher, respectively than those of sandwich-type). This indicates that there was another factor that affects the R_s in monolithic DSSC other than the length of the electron pathways in the counter electrode. Figure 1(b) shows that the counter electrode of monolithic DSSC is deposited on the FTO in one end and on the ZrO_2 layer on the other end, which resulted in one continuous layer but with a different height. A study by Luo *et al.* reported that a counter electrode deposited with unequal thickness may cause tensile stress at the peak and valley of the layer, thus causing possible cracks or disconnectivity between the counter electrode particles [42]. A crack could introduce large distances between particles, which consequently hampers the electron transport and increases the resistance in that region [43].

Regarding the charge transfer resistance at the counter electrode/electrolyte interface (R_{CE}), the sandwich-type DSSC with PEDOT:PSS counter electrode has the smallest R_{CE} (53 Ω), indicating that it has the best catalytic activity and the fastest electron transfer process among the other counter electrodes. For sandwich-type DSSC, the R_{CE} of the counter electrode with carbon composite (102 Ω) is higher than the R_{CE} of platinum (58,4 Ω). This could be caused by the morphology of the carbon counter electrode that is composed of large particle aggregates with plausible low surface area (see Figure 3(b)), thus causing relatively slow electron transfer. When comparing the cells based on their structure, it can be seen that the overall R_{CE} values for the monolithic type are much larger than the R_{CE} of the sandwich type. This indicates that the catalytic process in monolithic-type DSSC is much slower, and thus the electrolyte regeneration process is also slower. Similar to the sandwich-type DSSC, the R_{CE} of carbon composite counter electrode in the monolithic-type DSSC was also the lowest, providing the poorest catalytic activity than platinum and PEDOT:PSS.

The sandwich-type DSSC with platinum counter electrode has the highest C_{CE} (20.63 μF), indicating that more ions accumulated at the surface of the platinum counter electrode. Compared with the sandwich-type DSSC, the C_{CE} values of monolithic-type DSSCs are generally smaller, suggesting fewer ions accumulated at the counter electrode/electrolyte interface. Interestingly, regardless of the

structure, the PEDOT:PSS counter electrode shows relatively small C_{CE} (i.e. 1.05 μF), which suggests that the nonporous and low surface area owned by the PEDOT:PSS had possibly lowered its ability to accumulate ions on its surface.

The electrolyte diffusion resistance (R_d) could be affected by the size of the redox species, the viscosity of the electrolyte, and the concentration of redox species in the electrolyte [44]. Since the electrolytes used in this study are the same, the difference of R_d value is mostly affected by the counter electrode materials. The R_d values of sandwich-type DSSC are significantly lower than the R_d values of monolithic-type DSSC. This indicates that the diffusion of redox couples in DSSC with sandwich configuration occurred faster. One of the possible causes of the high R_d in monolithic-type DSSC is the high R_{CE} . Slow electron transfer from the counter electrode causes less amount of electrons that able to reduce I_3^- to I^- , thus less I^- ions diffused in the electrolyte. Furthermore, the addition of the ZrO_2 spacer layer in monolithic DSSC also contributes to the increase of diffusion resistance as less electrolyte volume could be allocated among the solid spacer layer [6, 13].

The difference in R_t for each variation of samples indicates that both configurations and the type of counter electrodes in DSSC could affect the electron transport process in TiO_2 . In addition to having the best catalytic activity as indicated by the smallest R_{CE} value, the PEDOT:PSS counter electrode on the sandwich-type DSSC produced the lowest R_t value that indicates the fast electron transfer process in the TiO_2 photoanode. The R_t value has a proportional effect on the electron transport time which can be expressed as [47]:

$$\tau_{tr} = R_t C \mu \quad (2)$$

DSSCs with good electrochemical performance ideally should have a low τ_{tr} value. The sandwich-type DSSC overall produced relatively low τ_{tr} values, which suggests that the transport electron in TiO_2 of sandwich-type DSSC is typically faster than that of monolithic-type DSSC.

The R_r value corresponds to the recombination resistance that occurs in the interface of dye/ TiO_2 /electrolyte. During impedance measurement under an open circuit, there are photoelectrons injected from the TiO_2 conduction band to the FTO substrate. All of the injected electrons are therefore contributed to the recombination process [45]. Thus, it could be stated that the recombined electrons are the electrons injected in the TiO_2 ($J_{\text{injection}} = J_{\text{recombination}}$). The R_r of sandwich-type DSSC with PEDOT:PSS counter electrode is the lowest among the other variations, indicating that there are more photoelectrons injected in the TiO_2 photoanode. The overall R_r of monolithic-type DSSC are much higher indicates that there are just a few photoelectrons injected. This phenomenon could be attributed to the poor catalytic activity, which hinders the dye regeneration process and consequently lowering electrons' injection into TiO_2 .

The ratio of recombination resistance and transport resistance is a parameter to determine the charge collection efficiency in TiO_2 . The ratio is determined from the electron diffusion distance (L_n), which is expressed as follows:

$$L_n = d \sqrt{\frac{R_r}{R_t}} \quad (3)$$

where d in equation 3 represents the thickness of TiO_2 (i.e. $\sim 10 \mu\text{m}$) and L_n is the average distance of electron diffusion before recombination. The L_n values of sandwich-type DSSC are overall higher than monolithic-type DSSC, wherein the highest L_n was obtained by the sandwich-type DSSC with

PEDOT:PSS counter electrode. As such, the current density generated by the sandwich-type DSSC with PEDOT:PSS counter electrode was also the highest among other variations. In contrast, the monolithic-type DSSC with platinum and carbon counter electrodes have shorter L_n compared with the thickness of TiO_2 . This causes more electrons to recombine than passing through the TiO_2 layer, hence less current could be generated.

Figure 6 shows the IPCE spectra of sandwich- and monolithic-type DSSC with platinum, carbon, and PEDOT:PSS counter electrode. The overall IPCE spectra show pronounce light absorption in two regions, i.e. under ultraviolet (UV) and visible light range. The first peaks occurring around 340 nm corresponds to the light absorption by TiO_2 that is associated with its bandgap (~ 3.2 eV). Meanwhile, the second peak formed at around 500 nm is associated with the peak absorption of the ruthenium Z907 dye. The light absorption of Z907 occurs in a longer wavelength due to its smaller bandgap of ~ 1.5 eV, so the energy required to excite the electrons is smaller than TiO_2 [46].

The IPCE value of DSSC relies on the probability of the light absorbed by the dye, the number of electrons excited by the dye into the TiO_2 conduction band, and the number of electrons injected into the external circuit from the TiO_2 conduction band. For sandwich-type DSSC, Figure 6 shows there is no significant difference obtained in the first region of the IPCE spectra regardless of the counter electrode. However, the IPCE maxima in the visible light region show different results for sandwich-type DSSC with platinum, carbon, and PEDOT:PSS counter electrode (i.e. 36.5%, 36.8%, and 55.0%, respectively). Despite having a slightly higher absorption peak, the sandwich-type DSSC with carbon counter electrode shows lower IPCE than platinum in other wavelengths, thus the overall photoelectric response for carbon is still lower compared with platinum DSSC. The highest IPCE value obtained by sandwich-type DSSC with PEDOT:PSS counter electrode could be attributed to the good catalyst activity (low R_{CE}) so that it can accelerate the diffusion process in the electrolyte (low R_d), and accelerate the electrons regeneration in dye [47]. The electron regeneration in the dye will eventually affect the number of electrons excited from the dye to the conduction band of TiO_2 .

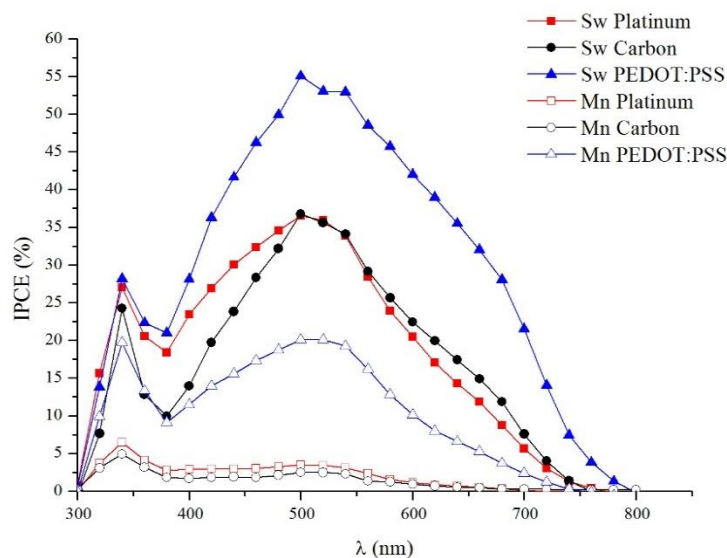


Figure 6. IPCE spectra of sandwich- (Sw) and monolithic-type (Mw) DSSC with platinum, carbon, and PEDOT:PSS counter electrode.

The IPCE graph in Figure 6 shows that the monolithic-type DSSC has a lower photoelectric response than the sandwich-type DSSC for all counter electrode variations. The low IPCE value of monolithic DSSC is probably due to dye absorption being less optimal in TiO_2 semiconductors. In contrast with sandwich-type DSSC where the TiO_2 layer surface was directly exposed to the dye during the sensitization process, during the fabrication of monolithic-type DSSC the TiO_2 layer was first coated with ZrO_2 and counter electrode layer, which made it more difficult for the dye to be absorbed by TiO_2 . Moreover, the addition of the ZrO_2 spacer layer also provides the additional electron transfer resistance from the electrolyte to the dye [8].

In the first region of the IPCE graph, the IPCE peaks of the monolithic-type DSSC show a value of 6.5%, 4.9%, and 19.7%, while at the second region the IPCE maxima were 3.5%, 2.2%, and 20.1% for platinum, carbon, and PEDOT:PSS counter electrode, respectively. These indicate that the light absorption of monolithic-type DSSC is mostly dominated by TiO_2 . The highest IPCE value for monolithic-type DSSC is shown by the sample with PEDOT:PSS counter electrode. This indicates that PEDOT:PSS has a good catalytic activity to accelerate the electrolyte reduction (low R_{CE}), and a good conductivity to transfer the electrons from the FTO substrate to the electrolyte (low R_{S}) allowing the dye to regenerate enough electrons to be injected into TiO_2 to continue the photoelectric cycles. The low IPCE values shown by the monolithic-type DSSC with carbon and platinum counter electrode could be attributed to the poor catalytic activity (high R_{CE}), which is not only hindering the electron regeneration in the dye but also hindering the electron regeneration at TiO_2 . In addition, the poor catalytic activity also increases the number of I_3^- ion in the electrolyte and increase the number of holes in the dye. Despite having some electrons in the TiO_2 valence band excited to the conduction band, those electrons will eventually recombine with I_3^- ions in the electrolyte or recombine with the holes in dye as indicated by the small L_{n} value. This makes it difficult for electrons to be injected into the substrate and external circuit, resulting in a small IPCE value.

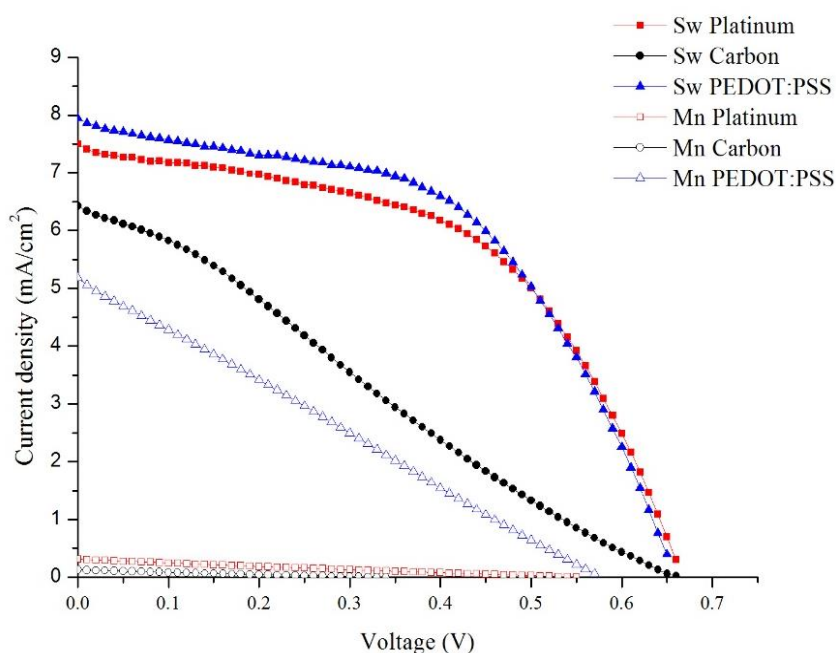


Figure 7. J-V characteristics of DSSC with the sandwich- (Sw) and monolithic-type (Mn) configuration with different variations of counter electrodes.

Table 3. Electrical parameters of sandwich [28] and monolithic DSSC with various counter electrodes.

DSSC type	PCE (%)	P_{\max} (mW)	V_{OC} (V)	J_{SC} (mA/cm ²)	FF
Sw Platinum	5.16	0.65	0.66	7.50	0.52
Sw Carbon	2.13	0.27	0.66	6.43	0.25
Sw PEDOT:PSS	5.40	0.68	0.65	7.95	0.52
Mn Platinum	0.08	0.01	0.55	0.31	0.23
Mn Carbon	0.04	0.01	0.34	0.13	0.22
Mn PEDOT:PSS	1.50	0.19	0.57	5.18	0.25

Comparison of the current density-voltage (J-V) curves between the sandwich- and monolithic-type DSSC with various counter electrodes is depicted in Figure 7 and the electrical parameters obtained are summarized in Table 3. Detailed electrical characteristics of the sandwich-type DSSC with various counter electrodes could be found in our previous study [28]. The variation of counter electrode material employed in both DSSC configurations has significant effects on the resulting electrical performance. Based on the shape of the J-V curves, Figure 7 shows that all of the monolithic-type DSSCs produced J-V curves that almost form a straight linear line, which is also confirmed by their lower fill factor values than the sandwich-type DSSC due to the high parasitic resistances. The fill factor of monolithic DSSC is lower than the fill factor of sandwich DSSC, due to the increase of R_s , R_{CE} , and R_d in monolithic DSSC. In addition, the structure of monolithic DSSC where the photoanode and the counter electrode are stacks up together increases the possibility of electron recombination from the TiO₂ conduction band to the counter electrode, which causes the decrease of shunt resistance and eventually decreases the fill factor. Overall, Table 3 shows that the cells with PEDOT:PSS counter electrode produced the highest PCE for both sandwich- and monolithic type DSSC. The highest performance was shown by the sandwich-type DSSC with PEDOT:PSS counter electrode with a PCE of 5.40%.

For sandwich-type DSSC, it is well understood that the V_{OC} does not vary significantly since there is no difference in the photoanode semiconductor used, the photoanode deposition method, and the type of electrolyte used. On the other hand, the PCE of the sandwich-type DSSC seems to be more determined by the J_{SC} . Besides having a close relationship with the photoelectric performance of TiO₂ and dye, J_{SC} also has a strong correlation with the activity of the counter electrode catalyst activity [3]. The cell with PEDOT:PSS counter electrode produced higher J_{SC} due to high catalytic activity, which results in the acceleration of electron transfer process from the FTO substrate to electrolyte through the PEDOT:PSS counter electrode. Even though Table 1 shows that the conductivity of PEDOT:PSS is 4.6 times higher than the conductivity of platinum, the sandwich-type DSSC with PEDOT:PSS counter electrode only produced slightly higher J_{SC} than that of platinum. This is possibly due to the surface structure of PEDOT:PSS that has a small roughness with nonporous nature, so that there are just a few active areas that could trap the electrolyte and transfer the electrons simultaneously [32]. Meanwhile, the lowest J_{SC} produced by the cell with carbon counter electrode is due to the characteristics of the composite paste that contains large aggregates and provides few activate areas to reduce the electrolyte. In terms of fill factor, Table 3 shows that the sandwich-type DSSC with PEDOT:PSS and platinum counter electrode has the same FF, while the carbon counter electrode has the lowest FF. The particle

structure that tends to agglomerate and uneven distribution of the particles causes an increase in R_{CE} that affects the reduction of I_3^- ions to I^- ions in the electrolyte. The slow ion reduction process causes the slow ion transfer process in the electrolyte, thereby increasing the ion transport resistance that also contributes to an increase in series resistance and a decrease in the FF of sandwich-type DSSC with carbon counter electrode.

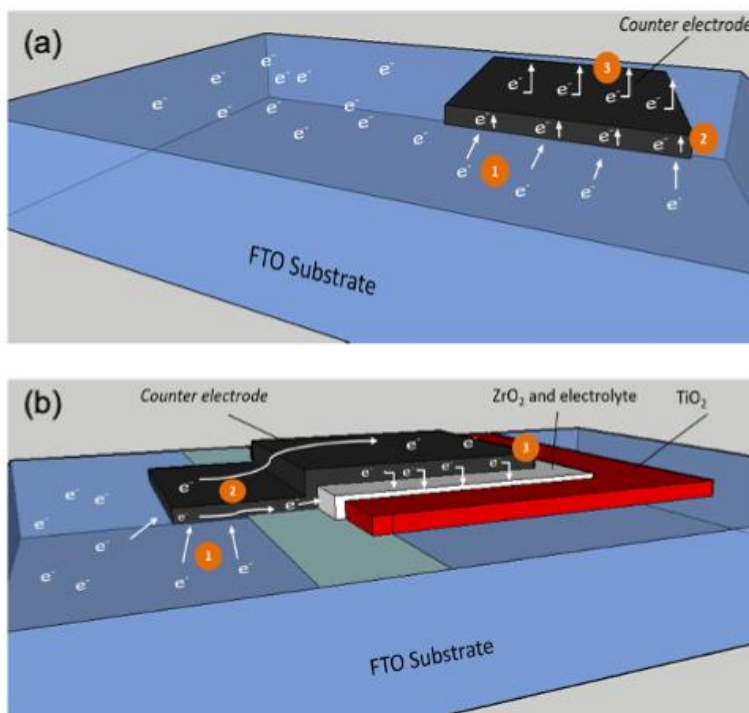


Figure 8. Illustration of the comparison between the electrons transport path in (a) sandwich- and (b) monolithic-type DSSC. The flows of electrons are labeled as follows: (1) electrons are transferred from the FTO substrate to the counter electrode; (2) electrons are transported across the counter electrode, and (3) electrons are transferred from the counter electrode to the electrolyte.

For monolithic-type DSSC, the V_{OC} values are overall lower than the V_{OC} of sandwich-type DSSC. This could be due to the configuration of the monolithic cell that only consists of one FTO substrate, with the photoanode and the counter electrode stacked on it. This form of configuration may risk electrons from the TiO_2 conduction band to recombine to the counter electrode without passing through the external circuit [38]. For this reason, the ZrO_2 spacer layer is typically added between the TiO_2 and the counter electrode. However, the low V_{OC} values suggest that the ZrO_2 with $\sim 4 \mu m$ thickness may not be able to completely prevent the recombination of TiO_2 to the counter electrode. Despite there was a decrease in V_{OC} for all monolithic-type DSSCs, the lowest V_{OC} was found on the sample with a carbon counter electrode. Apart from the fact that the ZrO_2 spacer layer does not completely prevent the recombination of electrons, another factor may be caused by the nature of the carbon composite layer that is less adhesive to the FTO substrates. This could lead to the attachment of carbon particles into the TiO_2 surface, blocking dye adsorption and thus lowering the V_{OC} . The J_{SC} values for the monolithic-type DSSC are also significantly lower than those of sandwich-type, particularly for those cells with carbon and platinum counter electrode. The role of the counter electrode as catalyst and electron

conductor will have a more significant effect on the DSSC performance with monolithic configuration than the sandwich. This is because the electron transport path in the counter electrode of sandwich DSSC is shorter than the electron transport path in the counter electrode of monolithic DSSC as illustrated in Figure 8. This explains why the J_{SC} in monolithic-type DSSC is proportional to the catalytic activity and conductivity of the counter electrode. For example, despite showing a good performance and catalytic activity in sandwich DSSC, platinum that has a lower conductivity than PEDOT:PSS produced higher R_S and R_{CE} . Thus, the monolithic-type DSSC with platinum produced lower J_{SC} than those with PEDOT:PSS counter electrode.

4. CONCLUSIONS

The effect of counter electrode materials on the electrochemical and electrical performance of sandwich- and monolithic-type DSSC have been systematically studied. The PEDOT:PSS counter electrode had a smooth surface structure with high conductivity of 3210 S/cm and produced the highest PCE of 5.40% when applied in sandwich-type DSSC. Similarly, the monolithic-type DSSC with PEDOT:PSS counter electrode produced higher PCE (i.e. 1.5%) than platinum and carbon. The outstanding performance of the DSSCs with PEDOT:PSS counter electrode was attributed to its high conductivity and low charge transfer resistance, thereby accelerating the regeneration of redox couples. DSSC with monolithic configuration overall produced lower performance than the DSSC with sandwich configuration partially due to an increase in series resistance as a result of long electron transport paths through the length of the counter electrode.

ACKNOWLEDGMENTS

The authors would like to thank the Materials and Devices for Solar Cells research group at the Research Center for Electronics and Telecommunication, Indonesia Institute of Sciences (P2ET LIPI), and Surya University for their assistance. EO and NMN are the main contributors to this paper. EO prepared the samples, collected the data, and wrote the paper; NMN led the project, designed the research, and wrote the paper; S and JH performed sample characterizations and cells fabrication; LMP and ESR reviewed the manuscript and provided administrative support for the project; while NP and GET involved in the discussion and contributed to the data analysis. Center for the Utilization and Innovation of Science and Technology at the Indonesian Institute of Sciences (PPII LIPI) and Institut Teknologi Bandung (ITB) are acknowledged for providing access to the SEM and EIS characterization facility, respectively. This work was partly supported by Program Riset Nasional Kemenristek/BRIN grant no. 141/E1/PRN/2020.

References

1. B. O'Regan and M. Gratzel, *Nature*, 353 (1991) 737.
2. D. Wei, *Int. J. Mol. Sci.*, 11 (2010) 1103.
3. M. Chen, L. L. Shao, B. A. C. Sulaiman, *Chem. Eng. J.*, 304 (2016) 629.
4. A. Andualem, S. Demis, *Edelweis Appli. Sci. Tech.*, 2 (2018) 145.
5. G. Hashmi, K. Miettunen, T. Peltola, J. Halme, I. Asghar, K. Aitola, M. Toivola, P. Lund, *Renewable Sustainable Energy Rev.*, 15 (2011) 3717.

6. N. M. Nursam, P. N. Anggraini, Shobih, J. Hidayat. Low-cost monolithic dye-sensitized solar cells fabricated on single conductive substrate, 2017 *International Conference on Radar, Antenna, Microwave, Electronics, and Telecommunications (ICRAMET)*, Jakarta, Indonesia, (2017) 164.
7. N. Papageorgiou, *Coord. Chem. Rev.*, 248 (2004) 1421.
8. J. Gong, J. Liang, K. Sumathy, *Renewable Sustainable Energy Rev.*, 16 (2012) 5848.
9. J. H. Wu, Z. Lan, J. M. Lin, M. L. Huang, Y. F. Huag, L. Q. Fan, G. G. Luo, Y. Lin, Y. M. Xie, Y. L. Wei, *Chem. Soc. Rev.*, 46 (2017) 5976.
10. M. X. Wu, T. L. Ma, *J. Phys. Chem.*, 118 (2014) 16727.
11. J. Briscoe, S. Dunn, *Adv. Mater.*, 28 (2016) 3802.
12. N M. Nursam, A. Istiqomah, J. Hidayat, P. N. Angggraini, Shobih, *Jurnal Elektronika dan Telekomunikasi*, 17 (2017) 30.
13. S. Ito, K. Takahashi, T. Yamaguchi, T. Komura, J. I. Nakamura, K. Murata, *J. Photoenergy*, (2012) 915352.
14. A. A. Arbab, K. C. Sun, I. A. Sahito, M. B. Qadir, Y. S. Choi, S. H. Jeong, *ACS Appl. Mater. Interfaces*, 8 (2016) 7471.
15. F. Arif, N. M. Nursam, N. Prastomo, Shobih, *J. Phys.: Conf. Ser.*, 1191 (2019) 01202.
16. S. Khodarimi, M. H. Hekhmatohar, M. Nasiri, M. M. Khaleghi Moghaddam, F. Abbasi, *J. Mater. Sci. – Mater. Electron.*, 27 (2015) 1278.
17. Y. L. Lee, C. L. Chen, L. W. Chong, C. H. Chen, Y. F. Liu, C. F. Chi, *Electrochem. Commun.*, 12 (2010) 1662.
18. A. Iefanova, U. Gautam, P. Poudel, D. Davouc, J. Nepal, V. Mallam, Q. Qiao, B. Louge, M. F. Baroughi, *IEEE 39th Photovoltaic Spec. Conf. (PVSC)*, (2013).
19. X. M. Fang, T. L. Ma, G. Q. Guan, M. Akiyama, T. Kida, E. Abe, *J. Electroanal. Chem.*, 570 (2014) 257.
20. S. J. Peng, F. Y. Cheng, J. F. Shi, Z. L. Tao, J. Chen, *Solid State Sci.*, 11 (2009) 2051.
21. M. X. Wu, X. Lin, T. H. Wang, J. S. Qiu, T. L. Ma, *Energy Environ. Sci.*, 4 (2011) 2308.
22. Y. G. Rong, Z. L. Ku, M. Xu, G. H. Liu, H. Wang, H. W. Han, *Front. Optoelectron.*, 6 (2013) 357.
23. J. G. Chen, H. Y. Wei, K. C. Ho, *Sol. Energy Mater. Sol. Cells*, 91 (2007) 1472.
24. D. Song, M. Li, F. Bai, Y. Li, Y. Jiang, B. Jiang, *Funct. Mater. Lett.*, 6 (2013) 1350048.
25. S. Edalati, A. Houshang, N. Torabi, Z. Baneshi, A. Behjat, *J. Phys. D: Appl. Phys.*, 50 (2016) 065501.
26. S. Thomas, T. G. Deepak, G. S. Anjusree, T. A. Arun, S. V. Nair, *J. Mat. Chem.*, A 2 (2014) 4474.
27. H. Petterson, T. Gruszecki, L-H. Johansson, P. Johander, *Sol. Energy Mater. Sol.*, 77 (2003) 405.
28. E. Oktaviani, N. M. Nursam, N. Prastomo, Shobih, *AIP Conf. Proc.*, 2232 (2020) 050001.
29. P. N. Anggraini, N. M. Nursam, Zulhayyir, Shobih, J. Hidayat, *AIP Conf. Proc.*, 2256 (2020) 060003.
30. N. C. D. Nath, A. Subramanian, R. Y. Hu, B. O. Lim, J. J. Lee, *J. Nanosci. Nanotechnol.*, 15 (2015) 8870.
31. P. Joshi, Y. Xie, M. Ropp, D. Galipaeu, S. Bailey, Q. Q. Qiao, *Energy Environ. Sci.*, 2 (2009) 426.
32. G. T. Yue, J. H. Wu, Y. M. Xio, J. M. Lin, M. L. Huang, *Chin. Sci. Bull.*, 58 (2013) 559.
33. D. Song, M. Li F. Bai, Y. Li, Y. Jiang, B. Jiang, *Funct. Mater. Lett.*, 6 (2013) 1350048.
34. C. T. Li, C. P. Lee, Y. Y. li, M. H. Yeh, K. C. Ho, *J. Mater. Chem.*, A 1 (2013) 1488.
35. Y. Huang, S. Dai, S. Chen, C. Zhang, Y. Sui, S. Xiao, L. Hu, *Appl. Phys. Lett.*, 95 (2009) 243503.
36. T. Ji, X. Hu, Y. Dai, Y. Chen, *Phys. Chem. Chem. Phys.*, 17 (2015) 4137.
37. Y. Jung, E. Stevens, B. Ding, S. D. Kim, S. K. Woo, J. K. Lee, *J. Mater. Sci.*, 48 (2013) 3760.
38. S. J. Thompson, N. W. Duffy, U. Bach, Y. B. Cheng, *J. Phys. Chem.*, C 114 (2010) 2365.
39. M. X. Wu, X. Lin, T. H. Wang, J. S. Qiu, T. L. Ma, *Energy Environ. Sci.*, 4 (2011) 2308.
40. L. Y. Han, N. Koide, Y. Chiba, T. Mitate, *Appl. Phys. Lett.*, 84 (2006) 2433.
41. Y. Hou, D. Wang, X. H. Yang, W. X. Fang, B. Zhang, H. F. Wang, G. Z. Lu, P. Hu, H. J. Zhao, H. G. Yang, *Nat. Commun.*, 4 (2013) 1583.

42. L. Luo, X. Zhang, Z. Zou, F. Guo, H. Qi, X. Zhao, P. Xiao, *J. Am. Ceram. Soc.*, 99 (2016) 3406
43. Y. Nishi, M. Hirano, *Mater. Trans*, 48 (2007) 2735.
44. Y. Y. Xiao, N. Chauhan, *Photoenergy and thin film materials*, Hoboken: Wiley & Sons (2019), Beverly, United States of America.
45. K. Subalakshmi, J. Senthilselvan, *Sol. Energy*, 171 (2018) 914.
46. S. Aghazada, M. K. Nazeruddin, *Inorganics*, 6 (2018) 1-34.
47. G. T. Yue, J. H. Wu, Y. H. Xiao, J. M. Lin, M. L. Huang, *Chinese Sci. Bull.*, 58 (2013) 559.

© 2021 The Authors. Published by ESG (www.electrochemsci.org). This article is an open access article distributed under the terms and conditions of the Creative Commons Attribution license (<http://creativecommons.org/licenses/by/4.0/>).